Line-focus-beam acoustic microscopy characterization of optical-grade LiTa03 single crystals

doi: 10.1063/1.373083

Line-focus-beam acoustic microscopy characterization of optical-grade $LiTaO_3$ single crystals

J. Kushibiki, T. Okuzawa, J. Hirohashi, and Y. Ohashi
Department of Electrical Engineering, Tohoku University, Sendai 980-8579, Japan

(Received 14 July 1999; accepted for publication 11 January 2000)

Basic data for evaluating homogeneities of $LiTaO_3$ single crystals for optical use are investigated by line-focus-beam acoustic microscopy. First, the relationships among leaky surface acoustic-wave (LSAW) velocities, chemical compositions, Curie temperatures, densities, and lattice constants are experimentally investigated as the calibration lines for crystal evaluation using *X*-, *Y*-, and *Z*-cut substrates prepared from three $LiTaO_3$ single crystals grown along the crystallographic *Y* axis with different Li_2O contents ranging from 48 to 49 mol %. It is shown that as the Li_2O content increases around the congruent composition, the LSAW velocities linearly increase for all specimen surfaces and all propagation directions, and the increase rate is maximum for *Z*-cut, *Y*-axis propagating (*ZY*) $LiTaO_3$. Next, homogeneities of the above three crystals and a commercially available optical-grade crystal are evaluated using *ZY*-$LiTaO_3$ specimens and the obtained calibration lines. The chemical composition variations along both the pulling direction and the diameter direction are successfully detected as LSAW velocity variations, due to the changes of crystal-growth conditions. In the commercial crystal, the LSAW velocity variations for the whole examined region (80 mm $\times$60 mm) exhibit a maximum difference of 0.82 m/s, corresponding to the composition change of 0.026 Li_2O mol %. It is demonstrated that this ultrasonic method has the unique and useful capabilities of detecting changes of the growth conditions and of evaluating local densities and the crystal-melt interface shape. © *2000 American Institute of Physics.* [S0021-8979(00)04808-8]

I. INTRODUCTION

$LiTaO_3$ (Refs. 1–5) is one of the most useful ferroelectric materials not only for surface acoustic-wave (SAW) devices because of its piezoelectric property, but also for optoelectronic devices because of its favorable acousto-optic, electro-optic, and nonlinear optical properties and high resistance to optical damage. Recently, one of the most important subjects of this crystal is to establish the growth conditions for producing large-diameter crystals with optically homogeneous properties. Chemical composition dependences of the refractive index, density, lattice constant, and Curie temperature have been investigated.[2,6–8] Also, it has been reported that the congruent composition of this crystal is about 48.5 mol % in Li_2O content.[3,5,8] However, it is not easy to grow homogeneous crystals because of its high melting point and generation of lattice imperfections. Therefore, it is necessary to precisely evaluate the lattice imperfections and compositional homogeneities and to feed back these results to adjust the growth conditions to resolve the above problems. $LiTaO_3$ crystals are conventionally evaluated by measuring the Curie temperature by differential thermal analysis (DTA),[2,3,6–8] the lattice constant and crystal imperfections by x-ray techniques,[2,7,9,10] the refractive index by the prism-coupler method,[2,7] the density,[2] and so on. Also, the chemical composition has been analyzed by inductively coupled plasma-atomic emission spectrometry (ICP-AES), electron probe microanalysis (EPMA), and x-ray fluorescence (XRF) analysis. However, these techniques still have some serious problems for conducting the research and development of optical-grade crystals with larger diameters and higher homogeneity. These problems include insufficient accuracy, destruction of the specimen, and very long measurement time. Therefore, although it is necessary to improve these conventional techniques, a technique that can perform nondestructive and noncontacting evaluation with higher accuracy should be developed. We have been proposing and demonstrating line-focus-beam (LFB) acoustic microscopy[11] as a technique to meet such requirements.

Materials are characterized by LFB acoustic microscopy by measuring the propagating characteristics, viz., phase velocity and attenuation, of leaky surface acoustic waves (LSAWs) (Ref. 12) propagating along one desired direction on a water-loaded specimen surface, through $V(z)$ curve analysis.[11] These measurements are very accurate, nondestructive, noncontacting, and speedy. We have applied LFB acoustic microscopy to the fundamental studies of $LiNbO_3$ and $LiTaO_3$ single crystals for SAW-device use and MgO-doped $LiNbO_3$ crystals for optoelectronic-device use.[13–16] For example, the area of partial multidomains in *X*-112° *Y* $LiTaO_3$ wafers, which results from an incomplete poling process, has been successfully detected as variations in LSAW velocity.[13] For 128° *YX*-$LiNbO_3$ and 36° *YX*-$LiTaO_3$ single crystals, the relationships among LSAW velocities, chemical compositions, and densities have been investigated.[14,15] These investigations have shown that the variations of chemical compositions and densities can be easily detected as variations in LSAW velocity. For MgO:$LiNbO_3$ single crystals, the relationships among LSAW velocities, chemical compositions, Curie temperatures, densities, lattice constants, and refractive indices have

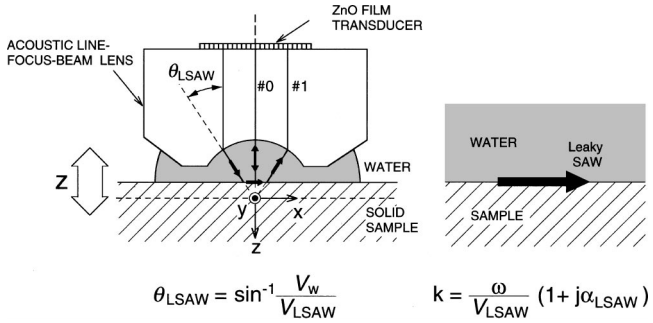

FIG. 1. Illustration of a cross section of a LFB acoustic device and a surface acoustic-wave mode for characterization. θ_{LSAW}: critical angle of LSAW, V_{LSAW}: LSAW velocity, and α_{LSAW}: normalized attenuation factor of LSAW.

been investigated, and it has been shown that measurement accuracy and resolutions of this ultrasonic method are better than any conventional evaluation method.[16]

The purpose of this article is to collect basic data for evaluating homogeneities of optical-grade $LiTaO_3$ single crystals and to establish the proper growth conditions by LFB acoustic microscopy. In particular, we will focus on the evaluation of compositional homogeneity, because of its close relationship with optical properties.[2,7] First, *X*-, *Y*-, and *Z*-cut substrates are prepared from three $LiTaO_3$ single crystals with different compositions ranging from 48 to 49 Li_2O mol %. LSAW velocities are measured for each crystal surface as a function of the wave propagation direction. Also, chemical composition dependences of LSAW velocities are investigated, and a proper crystalline plane and LSAW propagation direction suitable for crystal homogeneity evaluation are selected. Next, measured LSAW velocities are discussed in relation to the chemical compositions, Curie temperatures, densities, and lattice constants in order to quantitatively interpret measured velocities for crystal homogeneity evaluation. Further, homogeneities of the above crystals and a commercially available optical-grade single crystal are evaluated using the obtained calibration lines.

II. LFB SYSTEM

The method and system of LFB acoustic microscopy have been described in detail elsewhere.[11] Figure 1 shows the cross-sectional geometry of the LFB ultrasonic device and specimen system. Ultrasonic plane waves excited by the transducer are formed into a wedge-shaped ultrasonic beam by a cylindrical ultrasonic lens and focused on the specimen surface through water as a couplant. LSAWs are excited at the critical angle θ_{LSAW} and propagated along one selected direction on a water-loaded specimen surface. The propagation characteristics of the phase velocity and propagation attenuation are determined by analyzing a $V(z)$ curve, which is the interference wave form of two wave components of LSAWs (#1) and axial waves (#0), recorded as a function of the relative distance *z* between the LFB ultrasonic device and the specimen surface. The material is characterized by LSAW velocity measurements in this study, employing a sapphire cylindrical lens with a 1 mm radius and an ultrasonic frequency of 225 MHz. The propagation region of

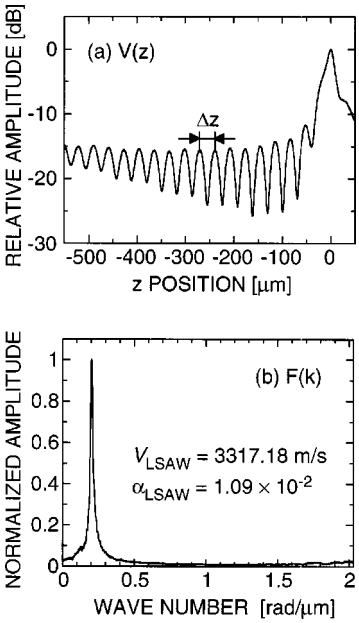

FIG. 2. Typical $V(z)$ curve measured for ZY-$LiTaO_3$ specimen at 225 MHz (a) and spectral distribution analyzed by FFT for the $V(z)$ curve shown above (b).

LSAWs is varied with about 7 μm (one wavelength in water) at the focal plane and about 550 μm at the 550 μm defocused position in length along the propagation direction (*x*-axis direction), and about 1 mm in 3 dB width along the unfocused direction (*y*-axis direction), as shown in Fig. 1. Measured LSAW velocity is the averaged one over this small region. Figure 2 shows the typical $V(z)$ curve measured for *Z*-cut, *Y*-propagating (*ZY*) $LiTaO_3$ and the spectral distribution analyzed by fast Fourier transform (FFT). According to the $V(z)$ curve analysis procedure,[11] and using the acoustic properties of pure water as the reference,[17] the phase velocity of LSAWs, V_{LSAW}, is determined with the oscillation interval Δz in the $V(z)$ curve as follows:

$$V_{\mathrm{LSAW}}=\frac{V_w}{\sqrt{1-\left(1-\frac{V_w}{2f\Delta z}\right)^2}},$$

where V_w is the longitudinal velocity of water, and f is the ultrasonic frequency. The most recent system, called the LFB ultrasonic material characterization (UMC) system,[18] is used in this study. This system can measure the LSAW velocity at 225 MHz with a relative accuracy better than $\pm 0.002\%$ at a chosen point and $\pm 0.004\%$ for two-dimensional scanning of 75 mm$\times$75 mm, and with an absolute accuracy of about $\pm 0.01\%$.[19]

III. SPECIMENS

A. Preparation

To quantitatively evaluate crystal homogeneities by LFB acoustic microscopy, it is necessary to investigate the relationship between LSAW velocities and chemical composition ratios to establish a calibration line. Therefore, three kinds of $LiTaO_3$ single-crystal ingots, termed crystals 1, 2,

TABLE I. Crystal-growth conditions and sizes of $LiTaO_3$ crystals.

Crystal No.	Prepared Li_2O content (mol %)	Pulling speed (mm/h)	Rotating speed (rpm)	Length (mm)	Diameter (mm)
1	48.0	7.11	8	68	77
2	48.5	7.22	8	66	77
3	49.0	7.33	8	67	77
C	Congruent	3.81	7	79	101

and 3, were grown from the melt of the starting materials of 48.0, 48.5, and 49.0 Li_2O mol %. A commercially available, optical-grade $LiTaO_3$ crystal (crystal C) with a nominally congruent composition was also prepared with an optional requirement of higher solidification to obtain a longer crystal. The crystal-growth conditions and sizes are summarized in Table I. These crystals, obtained from the Yamaju Ceramics Co., Seto, Japan, were grown along the crystallographic *Y*-axis direction by the Czochralski (CZ) technique. *X*-, *Y*-, and *Z*-cut substrates about 3 mm thick were taken as specimens from each crystal ingot, and prepared with both surfaces optically polished, as shown in Fig. 3. *Y*-cut substrates were taken at the middle position along the pulling direction. Figure 4 shows the configuration of each substrate. The crystal center line passes through the position marked by × on the *Y*-cut substrate. *Z*-cut substrates prepared were taken about 10 mm from the center. The × mark and dotted lines in Fig. 4 show the measurement positions for LSAW velocities and some other crystal properties in the following discussions.

B. Chemical composition

The physical properties depend upon the chemical composition ratios.[2,3,6–8] To obtain basic knowledge and data for characterizing crystal homogeneities and the growth conditions, it is fundamentally important to know the chemical composition ratios exactly. We conducted chemical composition analyses of crystals 1, 2, 3, and C using ICP-AES, which is useful for measuring Li and Ta concentrations, XRF analysis for Ta with the capability of stable measurements; and DTA, which is widely used for the composition analysis of $LiNbO_3$ and $LiTaO_3$ crystals. Other *Y*-cut specimens next to the specimens employed for velocity measurements were used for chemical analyses. The results are shown in Table II. In the results by ICP-AES, no significant differences in

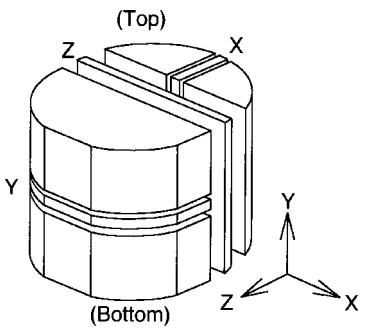

FIG. 3. Sample preparation.

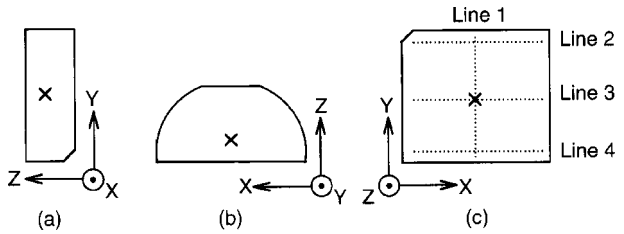

FIG. 4. Sample configurations and measurement positions of LSAW velocities and chemical and physical properties.

composition among the four crystals were observed. Furthermore, it is obvious that the analyzed values are less than the true values considering the result of the previous report[5,8] that the congruent composition must be close to 48.5 Li_2O mol %. The lower values may be due to the chemically insoluble properties of $LiTaO_3$, which prevent preparing a solution suitable for ICP-AES while maintaining the exact composition ratio. In XRF analysis, the intensities of fluorescent x rays for Ta in the crystals were measured. The proper differences in composition among them were probably not detected because the magnitudes of the differences were within the measurement errors. In DTA, the Curie temperatures were measured. As the prepared content of Li_2O increases, the Curie temperature increases monotonically. In our experimental investigation, we estimated the resolving power in DTA to be about ± 0.8 °C around 600 °C, and the chemical differences among the four crystals were clearly obtained. Therefore, the data of the chemical compositions obtained by DTA were used in this article. The Li_2O contents were determined from the measured Curie temperatures by using the relationship between the chemical compositions and Curie temperatures, which was reported by Sato *et al.*[8] These results are shown in Table III. The analyzed Li_2O contents approached the congruent composition (around 48.5 Li_2O mol %) as compared with the prepared Li_2O contents.[3,8] From this study, the chemical composition of crystal C, which is a commercially available $LiTaO_3$ crystal grown nominally with the congruent composition, was estimated to be around 48.52 Li_2O mol % at the middle of the crystal.

C. Densities and lattice constants

To continue the investigation, it is also necessary to know some other physical properties, as well as the chemical composition properties. The densities and lattice constants were, therefore, measured. The results are presented in Table

TABLE II. Results analyzed by ICP-AES, XRF analysis, and DTA.

Crystal No.	Prepared Li_2O content (mol %)	ICP-AES		XRF analysis	DTA
		Li_2O (mol %)	Ta_2O_5 (mol %)	Ta intensity (kcps)	Curie temp. (°C)
1	48.0	47.75	52.25	843.77	596.7
2	48.5	47.83	52.17	843.86	601.7
3	49.0	47.79	52.21	843.91	607.9
C	Congruent	47.76	52.24	844.07	602.5

TABLE III. Chemical and physical properties of the grown $LiTaO_3$ single crystals.

Crystal No.	Prepared Li_2O content (mol %)	Analyzed Li_2O content (mol %)	Curie temperature (°C)	Density (kg/m^3)	Lattice constant *a* (Å)	Lattice constant *c* (Å)
1	48.00	48.37	596.7	7463.4	5.154 08	13.784 35
2	48.50	48.50	601.7	7460.6	5.153 83	13.783 75
3	49.00	48.66	607.9	7457.9	5.153 63	13.783 22
C	Congruent	48.52	602.5	7460.7	5.153 82	13.783 74

III. Lattice constants *a* and *c* were measured for *X*- and *Z*-cut substrates by x-ray diffractometry using the Bond method.[20,21] These measurements were made at the positions marked by × in Fig. 4. Average densities were measured for *Y*-cut substrates by the Archimedes method.[22] As the Li_2O content increases, the Curie temperature increases monotonically, and the density and lattice constants decrease monotonically, as reported in previous works.[2,3,6,8] The change rates are $+38.8\,°C/Li_2O\,mol\,\%$ for Curie temperature, $-18.5\ (kg/m^3)/Li_2O\,mol\,\%$ for density, $-1.5\times10^{-3}\,Å/Li_2O\,mol\,\%$ for lattice constant *a*, and $-3.9\times10^{-3}\,Å/Li_2O\,mol\,\%$ for lattice constant *c*, from the linearly approximated lines using the least-squares method for the data of crystals 1, 2, and 3 in Table III.

IV. EXPERIMENTS AND DISCUSSIONS

A. Effect of chemical composition change on elastic properties

First, to examine the effect of compositional change on the elastic properties, we measured the angular dependences of LSAW velocities at the center of the *X*-, *Y*-, and *Z*-cut specimens of crystals 1, 2, and 3 at 225 MHz. All measured LSAW velocities were calibrated according to the LFB system calibration method using a gadolinium gallium garnet (GGG) (111) single crystal.[19] Figure 5 shows the results for each crystalline surface. The propagation directions of 0° and 90° for the *X*-cut specimens in Fig. 5(a) correspond to the *Y* and *Z* axes, respectively; those for the *Y*-cut specimens in Fig. 5(b), to the *X* and *Z* axes; and those for the *Z*-cut specimens in Fig. 5(c), to the *X* and *Y* axes. The velocities on each crystalline surface vary significantly with the propagation direction, reflecting the crystal symmetry, although the apparent LSAW velocity changes on the *X*-cut specimens were obtained in the range from 110° to 140°, due to the effect of another propagation mode (leaky psuedo-SAWs) (Refs. 12 and 23) on the present $V(z)$ curve analysis procedure.[11,12] Also, as the Li_2O content increases, the LSAW velocities increase monotonically for all propagation directions on each crystalline surface. The velocity increase rates due to the chemical composition change, calculated by the linear approximation, depend upon the propagation direction. The maximum value for the *X*-cut plane is $+24.5\ (m/s)/Li_2O\,mol\,\%$ in the 48.7° *Y* direction; for the *Y*-cut plane, $+23.8\ (m/s)/Li_2O\,mol\,\%$ in the *X*-axis direction; and for the *Z*-cut plane, $+30.9\ (m/s)/Li_2O\,mol\,\%$ in the *Y*-axis direction.

When this system is applied to evaluate crystal homogeneities, the propagation direction of LSAWs should be selected along the principle axes, or along the propagation direction, where the power flow angle becomes zero. Furthermore, the direction selected should be most sensitive to the chemical composition change. Considering these points, LSAWs propagating along the *Y*-axis direction on the *Z*-cut plane are most suitable for evaluating crystal homogeneity in the following investigations.

B. Calibration lines

The LSAW velocities on each *ZY*-$LiTaO_3$ shown in Fig. 5(c) were compared with the chemical and physical properties shown in Table III. Figure 6(a) shows the obtained relationship between the LSAW velocities and Li_2O contents; Fig. 6(b), Curie temperatures; Fig. 6(c), densities; and Fig. 6(d), lattice constants *a* and *c*. The straight lines shown in

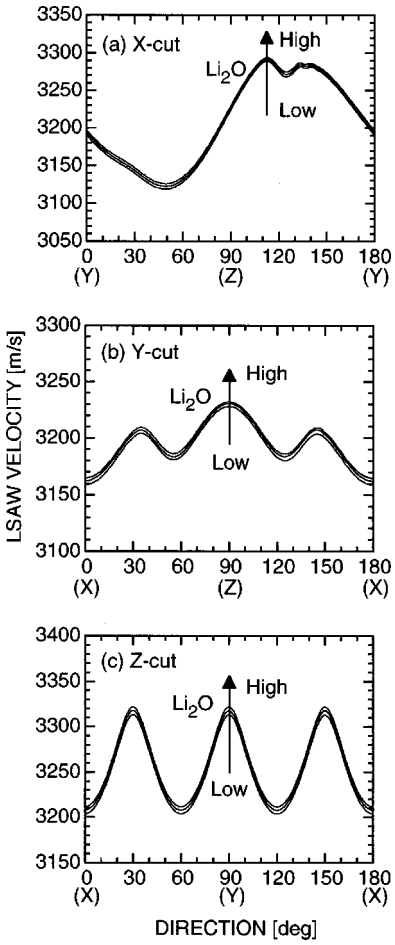

FIG. 5. Angular dependences of LSAW velocities for $LiTaO_3$ single crystals with different compositions.

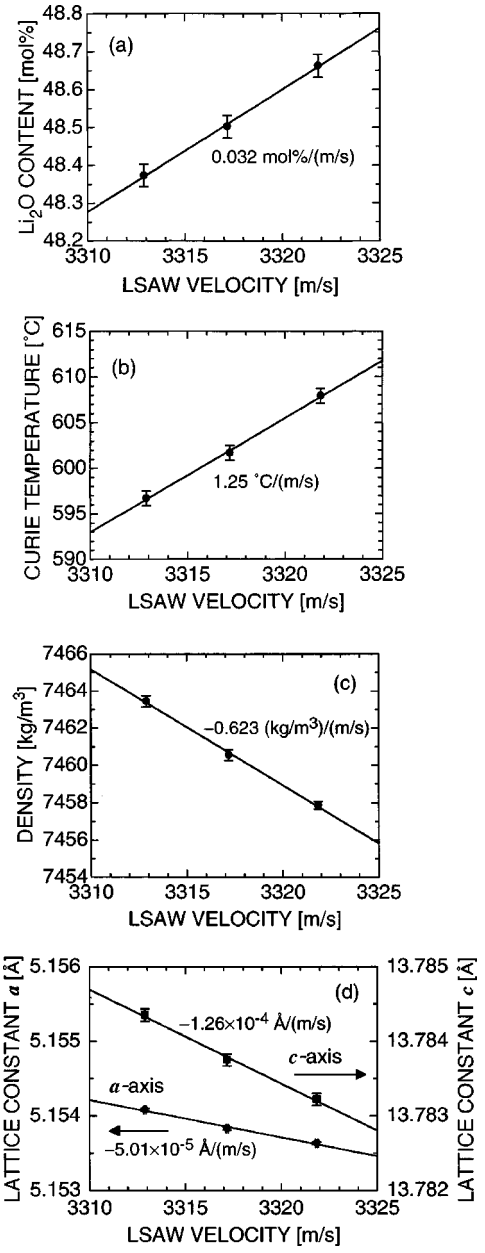

FIG. 6. Experimental relationships among LSAW velocities, Li_2O contents (a), Curie temperatures (b), densities (c), and lattice constants (d) for ZY-$LiTaO_3$ single crystals.

Figs. 6(a)–6(d) were calculated by linear approximation; the gradients in the same figures measure sensitivities of this ultrasonic method to the relevant properties. The relationships among the LSAW velocities and the above crystal properties were linear around the congruent composition, and the increase of LSAW velocity reflects the increase of Li_2O content and the decrease of density and lattice constant. Therefore, crystal homogeneities can be evaluated by measuring LSAW velocity variations in a crystal, and by using these relationships as the calibration lines. Table IV shows the measurement sensitivities and resolutions of this ultrasonic method for the chemical and physical properties of a $LiTaO_3$ single crystal. The resolutions were calculated from the obtained sensitivities and the relative accuracy for LSAW velocity measurements, $\pm 0.002\%$, corresponding to ± 0.07 m/s around 3300 m/s. This ultrasonic method should be a useful evaluation technique for developing and analyzing optical-grade $LiTaO_3$ single crystals because the sensitivity and resolution shown in Table IV are much better than those of the conventional methods, especially in quantitative detection of slight compositional variations of main atomic elements, viz., Li and Ta, in $LiTaO_3$ single crystals.

TABLE IV. Sensitivities and resolutions to chemical and physical properties for ZY-$LiTaO_3$ by LSAW velocity measurements.

	Sensitivity	Resolution
LSAW velocity	···	±0.07 m/s
Li_2O content	0.032 mol %/(m/s)	±0.002 mol %
Curie temperature	1.25 °C/(m/s)	±0.09 °C
Density	-0.623 (kg/m^3)/(m/s)	±0.04 kg/m^3
Lattice constant a	-5.01×10^{-5} Å/(m/s)	$\pm0.4\times10^{-5}$ Å
Lattice constant c	-1.26×10^{-4} Å/(m/s)	$\pm0.9\times10^{-5}$ Å

C. Evaluation of crystal homogeneities and growth conditions

1. Along the pulling axis

Using the obtained calibration lines, crystal homogeneities were evaluated by LFB acoustic microscopy. Here, we first directed our attention to homogeneities along the pulling direction because inhomogeneities in crystals grown by the CZ technique often occur along this direction and are of primary importance.

Samples 1, 2, 3, and C were Z-cut substrates prepared from each crystal as shown in Table I. LSAW velocities propagating along the Y-axis direction were measured in these four specimens in 1 mm steps along the pulling axis (line 1), as shown in Fig. 4(c). Figure 7 shows the results. In each crystal, the LSAW velocities varied linearly with the positions from the crystal top to the bottom. The change rates were obtained by linear approximation using the least-squares method. The rates are -0.02 (m/s)/mm for sample 1 and $+0.03$ (m/s)/mm for sample 3. The rate for sample 2 is less than $+0.01$ (m/s)/mm, having nearly the congruent composition, but the maximum velocity change for the distance of 40 mm is 0.39 m/s, which exceeds the velocity resolution of 0.07 m/s in this method. It is clear that there are some elastic variations. Those velocity variations are considered to

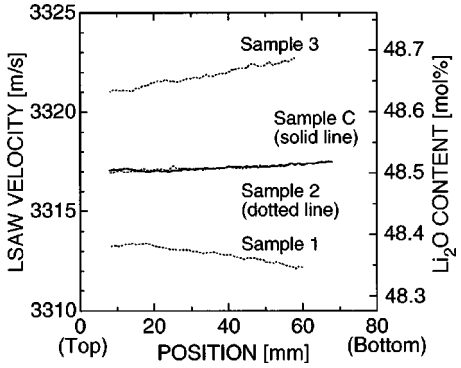

FIG. 7. LSAW velocity variations along the pulling axis for ZY-$LiTaO_3$ specimens with different compositions.

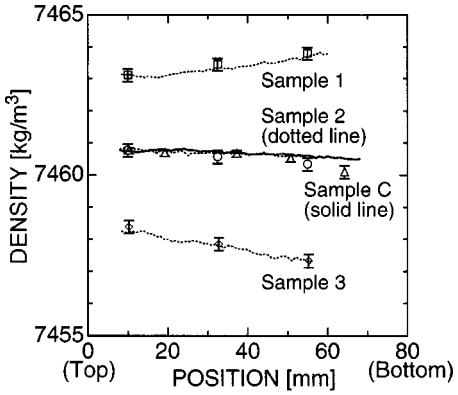

FIG. 8. Variations of measured and estimated densities along the pulling axis for $LiTaO_3$ single crystals with different compositions. Symbols indicate measured values; dotted and solid lines, estimated values from LSAW velocity variations shown in Fig. 7.

be evidence showing the detailed chemical composition variations in a crystal, referred to the calibration line shown in Fig. 6. The chemical composition ratios in the crystals from the upper parts to the lower parts vary linearly with change rates of -0.7×10^{-3} Li_2O mol %/mm for sample 1, $+0.2\times10^{-3}$ Li_2O mol %/mm for sample 2, and $+1.0\times10^{-3}$ Li_2O mol %/mm for sample 3. For sample C, the variations in LSAW velocity along the pulling-axis direction are quite similar to the results for sample 2 in Fig. 7, resulting in an almost monotonical increase from the upper parts of the crystal to the lower parts with a maximum deviation of 0.54 m/s (0.017 mol % in Li_2O concentration) and almost the same composition changing rate. The differences between the measurement values and the curves approximated by a third-order polynomial expression, applied to the four specimens, are less than ±0.15 m/s. These investigations thus revealed consecutive composition changes in the melt recorded in the crystal as acoustic variations along the pulling-axis direction.

These results also indicate the variations of densities and lattice constants along the *Y*-axis pulling direction, according to the interrelations among the LSAW velocities, densities, and lattice constants presented in Fig. 6.

To verify these evaluated results, we measured density variations along the pulling axis using the Archimedes method. Three *Y*-cut substrates from crystals 1, 2, and 3, and five *Y*-cut substrates from crystal C were selected at different positions in the crystal length direction shown in Fig. 3 and prepared as specimens. Figure 8 shows the results measured as the average value for the whole specimen, □ for crystal 1; ○, for crystal 2; ◇, for crystal 3; and △, for crystal C. The densities of crystal 1 increase from the top to the bottom with a maximum difference of 0.7 kg/m^3, while those for other crystals decrease with maximum differences of 0.4 kg/m^3 for crystal 2, 1.1 kg/m^3 for crystal 3, and 0.5 kg/m^3 for crystal C. Thus, even in the density measurements, the compositional variations in crystals are clearly detected along the pulling axis. This can be easily understood from the fact that the Li atomic weight of 6.941 differs largely from the Ta atomic weight of 180.9479. For comparison, the estimated density variations in the crystals along the pulling direction are presented in Fig. 8 as dotted lines for crystals 1, 2, and 3, and a solid line for crystal C, using the measured LSAW velocity variations in Fig. 7 and the calibration lines in Fig. 6(c). The measured density values agree well with the estimated values, and it is obvious that the LSAW velocity distributions presented in Fig. 7 correspond to the distributions of the chemical compositions and densities along the crystal pulling direction. This demonstrates that this ultrasonic method can evaluate density variations on the specimen in a small region.

Here, we discuss the relationship between the velocity variations in Fig. 7 and the crystal-growth conditions. In Fig. 7, the LSAW velocity variations observed can be understood as the Li_2O content variations. Considering that the composition ratio of a crystal depends on that of the melt, the chemical composition variations in Fig. 7 show that the melt composition was gradually changing while the crystal was growing. The cause of this change in the melt composition can be explained as follows. In Fig. 7, for sample 3 the Li_2O content around the position of 10 mm is estimated to be about 48.64 mol % and less than the melt composition of 49.0 mol %. This is because the crystal is going to grow so as to approach the congruent composition given in Table III, and means that Li_2O in the crystal growth was consumed at less than the prepared composition ratio. When the crystal is grown at the position 30 mm from the crystal top, the Li_2O content in the melt is considered to exceed 49.0 Li_2O mol %. In fact, the Li_2O content of the crystal grown at this position was estimated to be about 48.66 mol % and exceeded the Li_2O content of the crystal grown at 10 mm. It is interpreted that the Li_2O concentration in the melt gradually increases during the crystal growth so that the crystal contains more Li_2O concentration at the bottom parts than at the top parts.

In the case of sample 1, the Li_2O concentration in the melt gradually decreases during the crystal growth due to the opposite process, so that the crystal contains more Li_2O concentration at the top parts than at the bottom parts.

2. Along the diameter direction

Next, we try to examine the homogeneities of samples 1, 2, 3, and C along the diameter direction. LSAW velocities in the *Y*-axis propagation direction were measured in 1 mm steps along lines 2, 3, and 4 in Fig. 4(c). For each crystal, lines 2, 3, and 4 are selected for samples 1, 2, and 3 at the positions of 10, 32.5, and 55 mm from the top of the crystals, and for sample C at 10, 37, and 64 mm. The results are shown in Fig. 9. The dotted line in Fig. 9 shows the results obtained by the second- or third-order polynomial approximation. For each crystal, LSAW velocity changes in the whole crystal associated with the chemical composition variations, as seen in Fig. 7, were clearly observed depending upon the specimens and the positions, including the velocity changes along the pulling-axis direction. Concerning the velocity variations along the diameter direction, the velocities for sample 1 are greater around the center on all measurement lines with a convex shape in distribution. The same is true for sample 3 but with a concave shape, while velocities for sample 2 are less and almost flat as compared

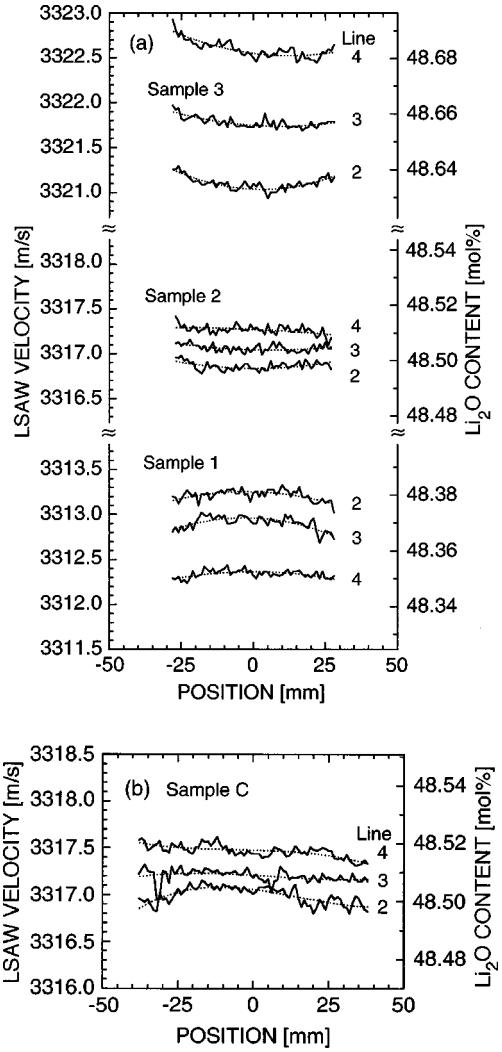

FIG. 9. LSAW velocity variations along diameter directions for ZY-$LiTaO_3$ specimens with different compositions. Solid lines indicate measured values; dotted lines, approximated curves.

with the other two samples. Considering that in the CZ technique a crystal is grown by rotating it and pulling it from the melt, it can be expected that the chemical composition changes during growth and the corresponding velocity variations exhibit nearly symmetrical distributions with respect to the position of 0 mm. However, we can see some asymmetric velocity variations for line 4 of sample 3 in Fig. 9. We suppose that those velocity variations reflect the shape of the crystal-melt interface during the growth.

We will now try to explain the process using the concave velocity distribution for line 2 of sample 3. We can assume, according to the literature,[24,25] that the crystal-melt interface shape was convex toward the melt just before crystal 3 at the position of line 2 was grown. The part that is first grown on line 2 is around the center of the crystal, near 0 mm; outer parts are gradually grown after that. Considering that the Li_2O content in the melt gradually increases during the growth of sample 3 as described above, it can be deduced that the Li_2O content in the melt becomes greater for the growth at the outer parts, so that the velocity variations measured on line 2 are greater at the outer parts with a concave shape. As we can similarly explain the velocity profiles for lines 3 and 4, the interface shape is supposed to be convex during the whole time of growing crystal 3 with the starting melt composition of 49.0 Li_2O mol %. Similarly, we can deduce from the velocity variations in Fig. 9 that, for crystal 1 with a starting melt composition of 48.0 Li_2O mol %, the crystal-melt interface shape was also convex toward the melt during the growth, but the degree of convexity at the interface depends upon the specimens and the positions because of the different velocity distributions shown in Fig. 9. In crystal growth by the CZ technique, the shape of the crystal-melt interface is mainly affected by the crystal rotation rate and crystal diameter, and crystals must be grown with a convex interface formed at a crystal rotation rate below the critical value, associated with a balance of natural and forced convection in melt.[24,25] Although the rotation rates of samples 1, 2, and 3 are the same as shown in Table I, the degree of convexity in the crystal-melt interface is different. This is caused primarily by the different melt compositions.

For sample C shown in Fig. 9(b), some interesting changes in the velocity profiles with rather complex shapes can be seen. The LSAW velocity profiles measured along lines 2, 3, and 4 remarkably differ from each other. The velocity distribution of line 2 has the large variations, especially around the positions -25 to $+10$ mm; that of line 3 is almost flat; and that of line 4 shows that the velocities gradually decrease to the right-hand side. The differences between the measured values and the approximated curves are within -0.27 to $+0.13$ m/s, which is greater than ± 0.1 m/s for line 1. It should be understood that there are not only relatively smooth composition variations as presented by the approximated curves, but also abrupt variations along the diameter direction, and that there are higher Li_2O concentrations, especially in the lower parts of the whole crystal. Considering that the measurements for lines 1–4 were performed at the same frequency on the same substrate surface, polished uniformly enough, and along the same wave propagation direction, the relatively greater velocity variations than the measurement resolution of 0.07 m/s should be interpreted here to be due to the chemical composition variations as a function of position, rather than problems such as surface damage introduced by the slicing and polishing processes. The LSAW velocities in lines 2–4 obtained for sample C are significantly different from those for sample 2, which has a chemical composition close to the congruent composition. Those slight velocity and profile changes might be evidence that some serious variations of the crystal-growth conditions occurred at the beginning. Further investigation is needed to confirm this.

D. Others

For sample C, the chemical composition distributions estimated from the velocity distributions measured for lines 1–4 are shown in Table V. The chemical composition changes along the diameter direction of the crystal are estimated to be 0.011 Li_2O mol % for line 2, 0.012 Li_2O mol % for line 3, and 0.010 Li_2O mol % for line 4. These values are less than the compositional distribution of 0.017 Li_2O mol %

TABLE V. Estimated variations of chemical and physical properties along the pulling axis [line 1 in Fig. 4(c)] and diameter directions [lines 2, 3, and 4 in Fig 4(c)] for crystal C.

	Line No.	LSAW velocity (m/s)	Li_2O content (mol %)	Curie temperature (°C)	Density (kg/m^3)	Lattice constant a (10^{-5} Å)	Lattice constant c (10^{-5} Å)
	1	0.54	0.017	0.68	0.34	2.7	6.8
Maximum	2	0.35	0.011	0.44	0.22	1.8	4.4
difference	3	0.38	0.012	0.48	0.24	1.9	4.8
	4	0.31	0.010	0.39	0.19	1.6	3.9
	All lines	0.82	0.026	1.03	0.51	4.1	10.3

in the pulling-axis direction (line 1). The slight LSAW velocity increase from the top to the bottom in Fig. 7 is quite similar to the measurements for $LiTaO_3$ crystals pulled along the *X* axis and the 36°-rotated-*Y* axis for SAW-device use.[26] These results for the four crystals suggest that the congruent composition to give a flat LSAW velocity distribution, which corresponds essentially to chemical composition homogeneity in the grown crystal, might contain slightly less Li_2O, about 48.48 mol %, as the starting material under the same growth conditions. Alternatively, the results may suggest that such subtle chemical variations may be associated with some special difficulties in the crystal-growth conditions of the CZ technique, especially for congruent $LiTaO_3$ which has a very high melting point of about 1620 °C. In any case, it is of great interest that the causes for the results shown in Figs. 7 and 9 might be related to the convection of the melt, the temperature and mechanical variations in the growing system, the shape of the crystal-melt interface during the growth, and other problems. However, further investigations into this anomaly are required.

The corresponding variations in Curie temperature, density, and lattice constant are presented in Table V. Their maximum deviations along the pulling axis are 0.017 mol % in Li_2O concentration, 0.68 °C in Curie temperature, 0.34 kg/m^3 in density, 2.7×10^{-5} Å in lattice constant *a*, and 6.8×10^{-5} Å in lattice constant *c*. For the whole examined area, the maximum variations are 0.026 mol % in Li_2O concentration, 0.51 kg/m^3 in density, and 1.03 °C in Curie temperature. According to Atuchin,[7] this Curie temperature change corresponds to 5.6×10^{-6} in the ordinary refractive index, and 1.2×10^{-4} in the extraordinary refractive index. To improve the inhomogeneity, it is necessary to detect such subtle chemical variations and to feed the information back to the growth conditions. However, such requirements are not satisfied by conventional analytical methods such as ICP-AES and XRF analyses, which cannot detect a difference of 0.3 Li_2O mol % in chemical composition between samples 1 and 3, as shown in sec. III B. The variations in the above also cannot be detected by the DTA method with a measurement resolution of ±0.8 °C or by the prism-coupler method with a resolution of $\pm2\times10^{-4}$ for the refractive index.[16] In contrast, this ultrasonic analytical method of measuring LSAW velocities has the major advantages of extremely high measurement sensitivity and resolution as given in Table IV; nondestructive and noncontacting evaluation; and very fast evaluation.

V. CONCLUSION

This study has applied the LFB-UMC system, which enables us to measure LSAW velocity very stably and accurately, to obtain basic data, and an experimental procedure for evaluating the homogeneity of $LiTaO_3$ crystals for optical use and for establishing the proper crystal-growth conditions. For this purpose, we prepared three $LiTaO_3$ single crystals with different melt compositions of 48.0, 48.5, and 49.0 Li_2O mol % and one commercially available optical-grade crystal, all of which were pulled along the crystallographic *Y* axis.

Using *X*-, *Y*-, and *Z*-cut specimens prepared from each crystal, LSAW velocities were measured and related to the other chemical and physical properties of chemical compositions, Curie temperatures, densities, and lattice constants. The chemical composition of the commercial crystal was estimated to be around 48.52 Li_2O mol %. It was shown that as the Li_2O content increases around the congruent composition, the LSAW velocities increase linearly for all the specimen surfaces and all the propagation directions, and that the *Y*-axis propagation on the *Z*-cut crystalline plane is suitable for crystal characterization because it has the highest velocity change rate.

With the calibration lines between the LSAW velocities and the other chemical and physical properties, the LFB-UMC system was applied to evaluate homogeneities of four *Z*-cut specimens of the above three crystals and one commercial crystal. Different composition variations from the crystal top to the bottom were observed along the pulling-axis direction, depending upon the melt compositions. Change rates were -0.7×10^{-3} Li_2O mol %/mm for the 48.0 Li_2O mol % melt composition, $+0.2\times10^{-3}$ Li_2O mol %/mm for the 48.5 Li_2O mol % melt composition, $+1.0\times10^{-3}$ Li_2O mol %/mm for the 49.0 Li_2O mol % melt composition, and $+0.2\times10^{-3}$ Li_2O mol %/mm for the commercial crystal. To grow homogeneous crystals in the pulling direction, the melt composition should thus be changed to around 48.48 Li_2O mol % under the same growth conditions for other parameters. Along the diameter direction, the velocity profiles varied clearly with the melt compositions: convex for the 48.0 Li_2O mol % melt composition, concave for the 49.0 Li_2O mol % melt composition, and almost flat for the 48.5 Li_2O mol % melt composition and commercial one which were close to the congruent composition. For the commercial crystal, a slight but significant

velocity distribution was observed. This might suggest some serious variations of the growth conditions while the crystal was growing. In this study, we succeeded in giving detailed interpretations of the crystal-growth processes with the different melt compositions, such as composition changes and crystal-melt interface shape during the growth, by measuring the LSAW velocities along the pulling-axis and diameter directions. The homogeneities of the commercial crystal were evaluated, and the compositional variations for the whole examined region ($80\,\mathrm{mm}\times 60\,\mathrm{mm}$) exhibited a maximum deviation of 0.026 $\mathrm{Li_2O\,mol\,\%}$.

The capability to evaluate the local density is very unique, and such an evaluation is impossible by any other technique. This ultrasonic method should be adopted as an analytical technique for establishing the crystal-growth conditions and processes, and for selecting and evaluating the wafers. Furthermore, it might provide solutions for other unresolved scientific and industrial material problems related not only to ferroelectric materials such as $LiTaO_3$ and $LiNbO_3$, but also to other materials such as nonpiezoelectric crystals and isotropic glasses.

ACKNOWLEDGMENTS

The authors are very grateful to T. Sasamata and I. Sahashi, Yamaju Ceramics Co., for growing the $LiTaO_3$ single crystals and measuring the Curie temperatures; Y. Okada, Kougakugiken Co., Ltd., for preparing the specimens; and K. Takada and M. Ishiguro, Institute of Materials Research, Tohoku University, for analyzing the chemical compositions by ICP-AES. This work was supported in part by a Research Grant-in-Aid from the Ministry of Education, Science and Culture of Japan.

[1] A. A. Ballman, J. Am. Ceram. Soc. **48**, 112 (1965).
[2] R. L. Barns and J. R. Carruthers, J. Appl. Crystallogr. **3**, 395 (1970).
[3] S. Miyazawa and H. Iwasaki, J. Cryst. Growth **10**, 276 (1971).
[4] C. D. Brandle and D. C. Miller, J. Cryst. Growth **24/25**, 432 (1974).
[5] T. Fukuda, S. Matsumura, H. Hirano, and T. Ito, J. Cryst. Growth **46**, 179 (1981).
[6] T. Yamada, N. Niizeki, and H. Toyoda, Jpn. J. Appl. Phys. **7**, 298 (1968).
[7] V. V. Atuchin, Opt. Spectrosc. **67**, 771 (1989).
[8] M. Sato, A. Iwata, J. Yamada, M. Hikita, and Y. Furukawa, Jpn. J. Appl. Phys., Part 1 **28**, 111 (1989).
[9] S. C. Abrahams and J. L. Bernstein, J. Phys. Chem. Solids **28**, 1685 (1967).
[10] S. Yasuami and T. Fukuda, J. Cryst. Growth **57**, 570 (1982).
[11] J. Kushibiki and N. Chubachi, IEEE Trans. Sonics Ultrason. **SU-32**, 189 (1985).
[12] J. J. Campbell and W. R. Jones, IEEE Trans. Sonics Ultrason. **SU-17**, 71 (1970).
[13] J. Kushibiki, H. Takahashi, T. Kobayashi, and N. Chubachi, Appl. Phys. Lett. **58**, 893 (1991).
[14] J. Kushibiki, H. Takahashi, T. Kobayashi, and N. Chubachi, Appl. Phys. Lett. **58**, 2622 (1991).
[15] J. Kushibiki, H. Ishiji, T. Kobayashi, N. Chubachi, I. Sahashi, and T. Sasamata, IEEE Trans. Ultrason. Ferroelectr. Freq. Control **42**, 83 (1995).
[16] J. Kushibiki, T. Kobayashi, H. Ishiji, and N. Chubachi, Appl. Phys. Lett. **61**, 2164 (1992).
[17] W. Kroebel and K. H. Mahrt, Acustica **35**, 154 (1976).
[18] J. Kushibiki and Y. Ono (unpublished).
[19] J. Kushibiki and M. Arakawa, IEEE Trans. Ultrason. Ferroelectr. Freq. Control **45**, 421 (1998).
[20] W. L. Bond, Acta Crystallogr. **13**, 814 (1960).
[21] J. Kushibiki, J. Hirohashi, and M. Arakawa (unpublished).
[22] H. A. Bowman and R. M. Schoonover, J. Res. Natl. Bur. Stand., Sect. C **71**, 179 (1967).
[23] K. Yamanouchi and K. Shibayama, J. Appl. Phys. **43**, 856 (1972).
[24] S. Matsumura, J. Cryst. Growth **51**, 41 (1981).
[25] J. Trauth and B. C. Grabmaier, J. Cryst. Growth **112**, 451 (1991).
[26] J. Kushibiki, Y. Ono, and I. Takanaga, IEICE Trans. Electron. **J82-C-I**, 715 (1999).